Digest Journal of Nanomaterials and Biostructures Vol. 12, No. 3, July - September 2017, p. 941 – 949

CHARACTERIZATION OF VERTICALLY ALIGNED ZINC OXIDE NANORODS VIA A RAPID MICROWAVE-ASSISTED HYDROTHERMAL SYNTHESIS PROCESS

V. M. FLORES-SÁNCHEZ, A. I. DÍAZ CANO, L. M. RESÉNDIZ MENDOZA*
Sección de Estudios de Posgrado e Investigación, UPIITA, Instituto Politécnico Nacional, Ciudad de México, México

This study presents an approach for the synthesis of vertically aligned zinc oxide nanorods (NR-ZnO) via a rapid microwave-assisted, low-cost, low-temperature, and non-time-consuming hydrothermal process. Two types of substrates, silicon and ITO, were used to compare the growth of vertically aligned NR-ZnO over those substrates. All X-ray diffraction reflections of the NR-ZnO were found that they were consistent with the wurtzite P63 mc space group, and the obtained scanning electron microscopy images indicated an aspect ratio of ~ 4. The polymer poly (3-hexylthiophene) (P3HT) was added to the NR-ZnO using a spin-coating method to assemble a hybrid heterojunction. Morphological and optical characterizations were performed. The NR-ZnO samples showed their contribution on spectral absorption in the UV–Visible region.

(Received June 8, 2017; Accepted September 22, 2017)

Keywords: Zinc oxide, hydrothermal method, Solar cells, ZnO nanorods, P3HT.

1. Introduction

The zinc oxide (ZnO) nanostructures have several potential applications, including in optoelectronics [1–3]. ZnO has a direct bandgap of approximately 3.37 eV at room temperature and an exciton binding energy of 60 meV [4]. Thus, ZnO nanostructures can be used in sensors, light-emitting diodes, UV lasers, field-effect transistors, and solar cells [5–9]. Different ZnO crystal nanostructures such as nanoparticles, nanosheets, nanorods, and nanowires can be formed using various growth conditions. Nanowire and nanorod structures are widely applied in solar cells as their active layers promote electron transfer and enhance the solar cells' light-harvesting efficiencies, ZnO nanorods have a good mechanical strength and thermal and chemical stability [10, 11]. Several methods such as chemical vapor deposition, metal–organic chemical vapor deposition, pulsed laser deposition, and the vapor–liquid–solid method have been studied for controlled synthesis of ZnO nanorods (NR-ZnO) [11–16]. However, these methods are expensive and require complicated growth conditions (e.g., high temperatures, inert gases, and complex equipment). The hydrothermal growth method is more versatile, cheaper, and easier [17]. NR-ZnO can be formed hydrothermally at low temperature and atmospheric pressure; however, the process is time consuming.

Microwave-assisted hydrothermal synthesis is a rapid nanoparticle synthesis method. This technique has several advantages such as a thermal homogeneous transmission giving a quick volumetric heating of the reagents in short reaction periods and with a one-step synthesis. This speed is possible due to the fact that microwaves transfer energy directly to the reagents. Using this procedure, the processing time for the growth of the ZnO nanowires has been reduced to up to 1 min [18–20]. The microwave-assisted hydrothermal process has been used to synthetize NR-ZnO in nanopowder form [21-22]; however, there have been limited analyses of nanorods grown in a vertical orientation on silicon and indium tin oxide (ITO) substrates with good adhesion.

* Corresponding author: lresendiz@ipn.mx

In this study, we report a quick, easy, and cheap synthesis process of NR-ZnO by a microwave-assisted hydrothermal method with a 2.45 GHz commercial microwave oven operated at a power of 700 W; which has a minimum production of non-toxic side-products during the NR-ZnO synthesis. The growth substrate was silicon or ITO. After characterizing its morphology and optical properties, the synthesized NR-ZnO was combined with the organic polymer poly (3-hexylthiophene) (P3HT) to develop a NR-ZnO/P3HT hybrid heterojunction, which allows having an absorption range in the UV–visible region. Therefore, this hybrid heterojunction may have optoelectronic applications.

2. Experimental

First, a solution containing 10 mM of zinc acetate dihydrate (98%, Aldrich) and 13 mM of $(CH_3)_2CHOH$ (spectroscopic grade, Aldrich) was prepared and spin coated onto the silicon (sample S1) and ITO (sample S2) substrates at 2000 rpm for 30 s. Prior to spin coating, the substrates were cleaned by ultrasonic bath in acetone, 2-propanol, and bidistilled water for 10 min and dried using compressed air. Then, the substrates were annealed at 120°C for 1 min after each spin coating to enhance their adhesion. Each substrate was completely covered by applying from three to six layers. A uniform seed layer was obtained after four layers of spin coating without nucleation.

Afterwards, NR-ZnO was grown by immersing substrates S1 and S2 in a equimolar mixture of 25 mM zinc nitrate hexahydrate ($Zn(NO_3)_26H_2O$, Fermot) and hexamethylenetetramine ($C_6H_{12}N_4$, Sigma Aldrich) in 100 ml of bidistilled water and heating with a commercial microwave oven (2.45 GHz; power=700W) at normal atmospheric pressure; microwave heating was performed for 1–4 min.

Following that, the substrates were removed from the solution, immersed in bidistilled water, and dried using compressed air for 1 min. For crystallization, NR-ZnO was subjected to thermal annealing at 130°C for 18 h in an air atmosphere.

Finally, to form the heterojunctions, 10 mg of P3HT was dissolved in 1.5 ml of chlorobenzene. This solution was deposited onto the NR-ZnO after NR-ZnO growth by spin coating at 2000 rpm for 60 s, resulting in an average polymer layer thickness of 100–120 nm. (Fig. 1).

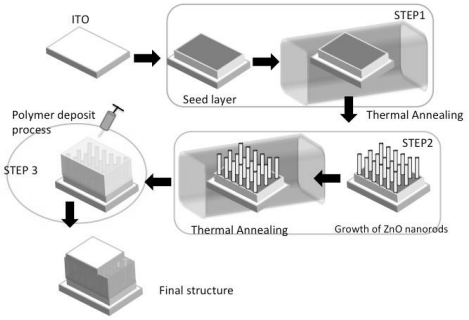

Fig. 1. Scheme of the NR-ZnO growth sequence

The surface morphology and size of the synthesized NR-ZnO were analyzed using a scanning electron microscope (SEM; Quanta 3DFEG-FEI) equipped with an energy-dispersive X-ray spectrometer (EDS; JEOL with Apollo X10 detector). The absorption spectrum of the NR-ZnO was recorded using a UV-Vis spectrophotometer (Shimadzu UV 2401PC). The refraction index and layer thickness of the NR-ZnO were measured using a variable-angle ellipsometer (Gaertner Scientific Corporation). The photoluminescence (PL) spectra of the NR-ZnO were measured at room temperature using a SPEX 500 spectrometer; the PL samples were excited by a He-Cd laser (wavelength = 325 nm) with a beam power of 80 nW. X-ray diffraction (XRD) patterns were

recorded with an XPERT MRD spectrometer with a pixel detector and a resolution of 0.00011. The X-ray beam was from the $K_{\alpha 1}$ line of a Cu source (λ = 1.5406 Å).

3. Results and discussion

An 81-nm thick uniform film of NR-ZnO was obtained after four layers were deposited by spin coating, and no nucleation was observed over the deposits on either S1 or S2.

The mechanism of NR-ZnO formation can be described as follows [23-25]. A homogeneous ZnO seed layer is grown on a conductive substrate (ITO or silicon) by spin coating. As shown in Eq. (1), (Zn $(CH_3COO)_2$ H_2O) is dissolved in 2-propanol and ZnO is precipitated as a thin layer:

$$Zn^{2+} + 2CH_3COO^- + 2OH^- + 2H^+ \rightarrow ZnO\downarrow + 2CH_3COO\uparrow + 2H_2O\uparrow \quad (1)$$

In the second step, aligned NR-ZnO is grown via a microwave-assisted hydrothermal method:

$$Zn^{+2} + 2OH^- \rightarrow Zn(OH)_2 \quad (2)$$

$$Zn(OH)_2 \rightarrow ZnO\downarrow + H_2O\uparrow \quad (3)$$

When the ZnOH concentration reaches the saturation point (2), ZnO precipitates (3), stimulating the growth of ZnO nanoparticles.

It has been suggested that using temperatures like 300°C for 1 h can improve the crystallization of NR-ZnO. Moreover, the morphology of the crystallized ZnO can be affected by the concentration, pH, and choice of microwave [26].

Under our growth conditions, vertically aligned hexagonal NR-ZnO was obtained on silicon and ITO substrates, as it is observed in the SEM images (Fig. 2). The typical width and length estimated from the SEM images are 20 nm and 80 nm, respectively, and the aspect ratio is approximately 4:1.

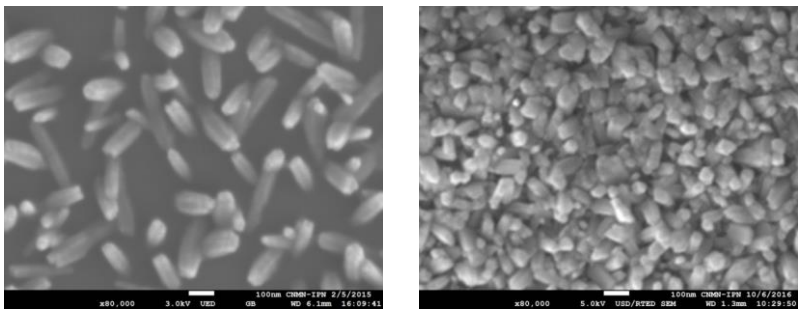

Fig. (2). SEM images of hexagonal NR-ZnO grown on (a) silicon and (b) ITO substrate at 700 W for 4 min in a commercial microwave oven

Figure 3 shows the EDS spectra of NR-ZnO grown on substrates S1 and S2. The elemental concentrations estimated by EDS are shown in Table 1 and the corresponding elements that compose the nanorods, as well as the substrates, are also indicated. It can be clearly observed in figure 3b that the corresponding peaks for the elements that compose NR-ZnO (Zn and O) and ITO (In and Sn) are presented; moreover, there is presence of Si. As the ITO layer is grown on a glass substrate, those elements are components of the substrate.

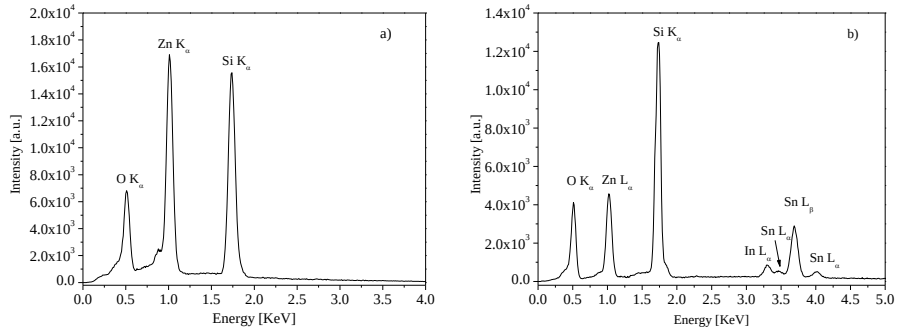

Fig. 3. EDS of NR-ZnO on (a) silicon (S1) and (b) ITO (S2)

Under the same crystallization conditions, the NR-ZnO density was higher on the ITO substrate than on the silicon substrate (Figs. 2a and 2b). This finding suggests that an irregular surface, such as ITO, is better for the adherence of the NR-ZnO seed layer than polish surface such as silicon. However, ITO is degraded at temperatures higher than 200°C under non-vacuum conditions, which could significantly modify the optical and electrical properties of ITO [27]. Thus, increasing the ZnO crystallization temperature may affect both the optical and electrical properties of our hybrid interface (ITO-NR-ZnO).

Table 1. Analysis of K-lines in EDS of elements ZnO.
EDS of ZnO on S1

Element	Weight %	Atomic %	Error %
O K_α	16.87	45.34	6.6
Zn L_α	53.08	24.61	4.9
Si K_α	28.05	30.05	5.51

EDS of ZnO on S2

Element	Weight %	Atomic %	Error %
Si K_α	59.9	80.06	1.53
O K_α	20.65	10.70	6.86
Z L_α	9.05	2.21	4.57
Sn L_α	5.86	5.1	5.34
In L_β	4.45	1.93	8.7

The measured XRD pattern of NR-ZnO grown on S1 (Fig. 4a) shows peaks at 31.78°, 34.43°, 36.29°, 47.56°, 56.67°, 62.90°, and 67.99°, corresponding to the (100), (002), (101), (102), (110), (103), and (112) planes, respectively, of the wurtzite ZnO crystal lattice (JCPDS 36-1451). These characteristic peaks were also observed in the pattern of the NR-ZnO grown on the ITO substrate (Fig. 4b). The ITO peak was identified according to JCPDS 6-416 based on the high-intensity (222), (440), and (622) reflection in the standard pattern. ZnO has Wurzite structure, and its growth is to close packed planes and with low energy as (002).

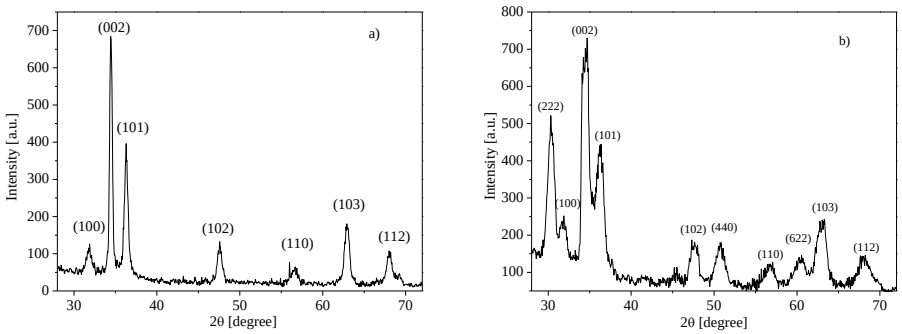

Fig. (4). XRD patterns of NR-ZnO grown on (a) silicon substrate (S1) and (b) ITO substrate (S2)

The crystalline quality from NR-ZnO grown over silicon substrate (S1) is higher than NR-ZnO grown on ITO substrate (S2) as it observed the characteristic signals (peaks) from XRD in figure 4. However, a higher density of growth per superficial area was obtained when NR-ZnO were growth on S2 than on S1 (Fig. 2)

From the XRD patterns, the crystallite size was measured along the (002) plane using Schreer's formula [28]:

$$D = \frac{K\lambda}{\beta \cos\theta} \tag{4}$$

where D is the crystal size or grain size, λ is the X-ray wavelength of the incident Cu K_α radiation (0.154056 nm), *K* is a dimensionless shape factor that typically takes the value of 0.9 for spherical crystallites, β is the line broadening at half the maximum intensity after subtracting the instrumental line broadening (in radians), and θ is the Bragg angle. The ZnO crystallite sizes were determined to be 19.73 nm for S1 and 8.74 nm for S2.

The PL spectra of the annealed NR-ZnO samples are shown in Fig. 5. It is clear that the PL spectra are complex and can be represented by superposition of sets of PL bands. A deconvolution procedure was applied to the obtained PL spectra (Fig. 5a), resulting in at least five elementary PL bands with peaks at 390, 409, 568, 650, and 770 nm for S1. The elementary PL bands at 568 and 650 nm were previously attributed to defect-related emissions in ZnO nanosystems [29-31], and the orange PL band at 554–650 nm was attributed to interstitial oxygen atoms (650 nm) [32] or hydroxyl groups (568 nm) [33,34]. As the density of the NR-ZnO increases (Fig. 5b), the intensities of the defect-related PL peaks also increase, apparently as a result of the increased density of NR-ZnO. These defects are mainly located in the interfacial region between the NR-ZnO and the ITO glass. The PL intensity also increases with increasing defect density. In this study, the intensities of the PL bands for the S2 sample increase with NR-ZnO density. In contrast, for the ITO (S2) substrate, no characteristic PL peaks of NR-ZnO were evident, as shown in Fig. 5b. They were probably masked by the substrate ITO (419, 554, and 700 nm [35-38]. Similar results were reported in [39]. They found that by using low precursor concentrations, the PL spectra of the NR-ZnO were mainly dominated by characteristic peaks from the substrates. When the precursor concentration is higher, the contribution from NR-ZnO in the PL spectra becomes dominant.

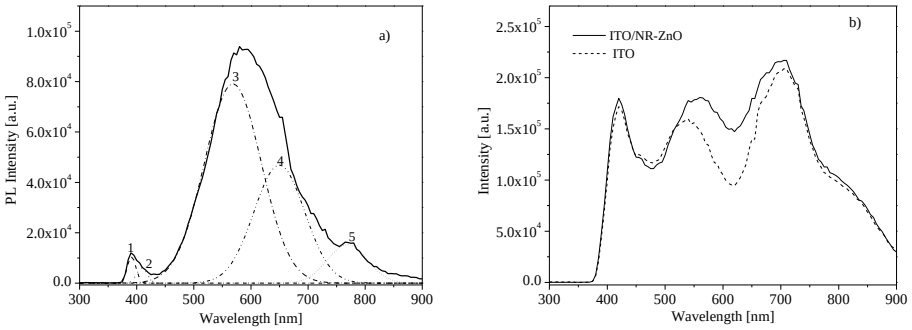

Fig. 5. PL spectra of NR-ZnO grown on (a) silicon substrate (S1) and (b) ITO substrate (S2)

To examine the optical properties of NR-ZnO, the absorbance curves of the NR-ZnO samples were obtained. Figure 6 shows the absorption spectrum of NR-ZnO on glass/ITO (S2); absorbance is observable in the range of 304–392 nm with a peak at 358 nm, indicating strong absorbance in the UV region, as is characteristic of ZnO.

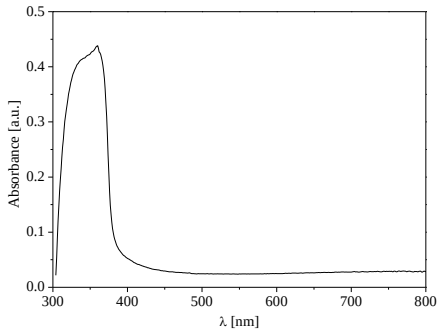

Fig. (6). Absorbance curve of NR-ZnO on ITO (S2)

The optical band gap was obtained by plotting $(\alpha hv)^2$ as a function of photon energy (hv). The intercept of the extrapolation to zero absorption on the photon energy axis gave the direct energy gap (Eg) [40-41]. Figure 7 presents the Tauc analysis results for NR-ZnO grown on S2, given an optical band gap around 3.28 eV and a thickness of 80 nm. These results are similar to those in other reports [42-43].

The above can be corroborated through the photoluminescence spectra of NR-ZnO growth on silicon (S1) (Figure 5a) where the start of the peak emissions due to excitonic recombination at 375 nm, corresponding to an optical band gap of 3.3 eV.

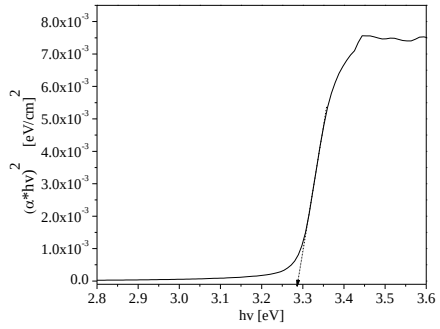

Fig. 7. Tauc plot of NR-ZnO grown on ITO (S2)

Once a homogeneous and uniform layer of NR-ZnO was obtained, a polymer layer was added. P3HT was chosen for its relatively high hole mobility and because it is the most widely semiconductor organic used in different optoelectronic applications [44]. P3HT was added after the NR-ZnO samples grown on silicon and ITO. The SEM images (Fig. 8) illustrate the distribution of P3HT among the NR-ZnO structures. P3HT exhibits greater adherence to NR-ZnO when structures are grown on ITO substrates; the absorbance curve (Fig. 9) confirms the presence of both NR-ZnO and P3HT. This hybrid interface exhibits absorption profile enhancement in the UV and visible regions, with two major absorption peaks at 350 nm and 550 nm

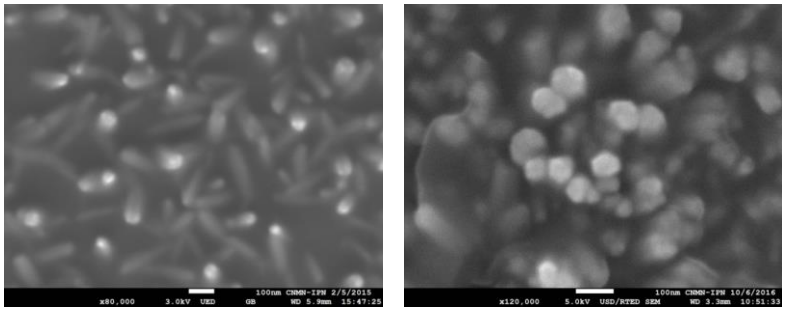

Fig. 8. SEM images of NR-ZnO with P3HT (a) Si-NR-ZnO-P3HT and (b) ITO-NR-ZnO-P3HT

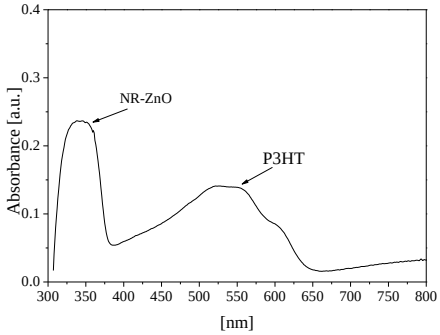

Fig. 9. Absorbance curve of NR-ZnO on ITO (S2) with P3HT

3. Conclusions

We synthesized vertically aligned NR-ZnO on silicon and ITO substrates and examined their morphologies and optical properties. XRD analysis revealed that we obtained NR-ZnO arrays of high-quality crystals. The natures of radiative defects were clarified for some PL bands (554, 650, and 568 nm). As a result of the PL analysis, a novel synthetic route for high-purity hexagonal NR-ZnO reported herein enables emission, from the excitonic band (375 - 435 nm) to the defects band (375 - 435 nm) on a silicon substrate. However the characteristic peaks of NR-ZnO on the ITO substrate is masked by a PL spectrum of the substrate. Moreover, the PL intensity was enhanced in the sample grown on the ITO substrate due to an increase in the NR-ZnO density, which increased the defect density in the interfacial regions between NR-ZnO and the ITO glass. Also, the heterojunction between NR-ZnO and the polymer P3HT gave a broad absorption spectrum covering from the UV to the visible regions. This result suggests a wide range of possible applications of this heterojunction in optoelectronics, such as solar cells. Therefore, NR-ZnO grown over both ITO and silicon substrates can have applications in optoelectronic devices.

Acknowledgments

This work was supported by the SIP-IPN project 20171781. V.M. Flores-Sanchez received a grant from CONACYT, Mexico. We thank the Department of Electrical Engineering, Section of Solid-State Electronics, CINVESTAV-IPN, Mexico for letting us use its facilities and the CNMN-IPN, Mexico for SEM measurements.

References

[1] S. Muthukumar, H. Chen, J. Zhong, Z. Zhang, N. W. Emantoglu, Y. Lu, IEEE Trans. Nanotech. **2**, 50 (2003).
[2] A. I. Díaz Cano, B. El Filali, T. V. Torchynska, J. L. Espinola. J. Phy. Chem. Solids **74**, 431 (2012).
[3] C. Jagadish and S. J. Pearton. Zinc Oxide Bulk, Thin Films and Nanostructures, 1st ed. Elsevier, New York (2006).
[4] U. Ozgur and Y. I. Alivov, J. Appl. Phys. **98**, 041301 (2005).
[5] Q. Wan, Q. H. Li, Y. J. Chen, T. H. Wang, X. L. He, J. P. Li, C. L. Lin. Appl. Phys. Lett. **84**, 3654 (2004).
[6] C. H. Liu, J. A. Zapien, Y. Yao, X. M. Meng, C. S. Lee, S. S. Fan. High-Density, Adv. Mater. **15**, 838 (2003).
[7] Z. K. Tang, G. K. L. Wong, P. Yu, M. Kawasaki, A. Ohtomo, H. Koinuma, Y. Segawa. Appl. Phys. Lett. **72**, 3270 (1998).
[8] M. S. Arnold, P. Avouris, Z. W. Pan, Z. L. Wang. J. Phys. Chem. B. **107**, 659 (2003).
[9] B. Pradhan, S. K. Batabyal, A. J. Pal, Sol. Energy Mater Sol. Cells. **91**,769 (2007).
[10] R. Shenqiang, C. Liang-yi, L. Sung-keun, Z. Jing. Nano Lett. **11**, 3998 (2011).
[11] R. J. H. Morris, M. G. Dowsett, S. H. Dalal, D. L. Baptista, K. B. K. Teo, W. I. Milne, Surf. Interface Anal. **39**, 898 (2007).
[12] W. Lee, M. C. Jeong, J. M. Myoung, Acta. Mater. **52**, 3949 (2004)**.**
[13] Y. Zhang, R. E. Russo, S. S. Mao, Appl. Phys. Lett. **87**, 133115 (2005).
[14] M. H. Huang, Y. Wu, H. Feick, N. Tran, E. Weber, P. Yang. Adv. Mater. **13**,113 (2001).
[15] M. J. Height, L. Madler, S. E. Pratsinis, F. Krumeich, Chem. Mater. **18**, 572 (2006).
[16] A. B. Djurisic, A. M. C. Ng, and X. Y. Chen, Prog. Quantum Elec. **34**, 191 (2010).
[17] L. Vayssieres, Adv. Mater. **15**, 464 (2003).
[18] G. M. B. Parkes, P. A. Barnes, G. Bond, E. L. Charsley, Thermochimica Acta **356**, 85 (2000).
[19] P. Benito and F. M. Labajar, Bol. Soc. Esp. Ceram. **43**, 56 (2004).
[20] M. L. Sheppard, Amer. Ceramic Soc. Bulletin. **67**, 1656 (1988).
[21] K. Ocakoglu, Sh. A. Mansour, S. Yildirimcan, A. A. Al-Ghamdi, F. El-Tantawy, F. Yakuphanoglu. Acta Mol. Biomol. Spectr. **148**, 362 (2015).
[22] H. Yu, H. Fan, X Wang, J. Wang. Optik- International Journal for Light and Electron Optics, **125**, 1461 (2014).
[23] G. Rodriguez-Gattorno and G. Oskam, ECS Trans. **3**, 23 (2006).
[24] Y. Zhang, M. K. Ram, E. K. Stefanakos, D. Y. Goswami, J Nanomater. **2012**, 1 (2012).
[25] S. Baruah,J. Dutta, J Sol-Gel Sci. Technol. **50**, 456 (2009).
[26] S. Komarneni, M. Bruno, E. Mariani, Mater. Res. Bulletin **35**, 1843 (2000).
[27] R. X. Wang, C. D. Beling, S. Fung, A. B. Djurisic, C. C. Ling, S. Li, J. Appl. Phys. **97**, 033504 (2005).
[28] H. W. Kim, N. H. Kim, Mater. Sci. Semicond. Process. **7**, 1 (2004**)**.
[29] A. M. C. Ng, X. Y. Chen. Prog. Quantum Elec. **34**, 191 (2010)
[30] T. Voss, C. Bekeny, L. Wischmeier, H. Gafsi, S. Borner, W. Schade, A. C. Mofor, A. Bakin, A. Waag. Appl. Phys. Lett. **89**, 182107 (2006).
[31] M. A. Reshchikova, H. Morkoc, B. Nemeth, J. Nause, J. Xie, B. Hertog, A. Osinsky. Physica B: Condensed Matter. **358**, 401 (2007).
[32] X. Liu, X. Wu, H. Cao, R. P. H. Chang. J. of Appl. Phys. **95**, 3141 (2004).

[33] J. Qiu, X. Li, W. He, S. -J. Park, H. -K. Kim, Y. -H. Hwang, J. -H. Lee, Y. -D. Kim. Nanotech. **20**, 155603 (2009).
[34] R. B. M. Cross, M. M. De Souza, E. Sankara Narayanan, Nanotech. **16**, 2188 (2005).
[35] Z. Sun, J. He, A. Kumbhar, J. Farg. Langmuir. **26**, 4246 (2010).
[36] S. Luo, S. Kohiki, K. Okada, F. Shoji, T. Shishido, Phys. Status Solidi A. **207**, 386 (2010).
[37] J. Gao, R. Chen, D. H. Li, L. Jiamg, J. C. Ye, X. C. Ma, X. D. Chen, Q. H. Xiong, H. D. Sun, T. Wu, Nanotech. vol. **22**, 195706 (2011).
[38] S. Kundu, P. K. Biswas, Chem. Phys. Lett. **414**, 107 (2005).
[39] F. Tong, K. Kim, Y. Wang, R. Thapa, Y. Sharma, A.Modic, A. Claude Ahyi, T. Issacs-Smith, J. Williams, H. Ahn, H. Park, D. J. Kim, S. Lee, E. Lim, K.K. Lee, M. Park. Growth of ZnO Nanorod Arrays on Flexible Substrates: Effect of Precursor Solution Concentration. ISRN Nanomater. **7**, 2012.
[40] F.E. Ghodsi, H. Absalan. Acta Physica Polonica A. **118**, 559 (2010).
[41] B. D. Viezbicke, S. Patel, B. E. Davis, P. Dunbar, Phys. Status Solidi B, **8**, 1700 (2015).
[42] M. H. Manat, Z. Khusaimi, M. Z. Musa, M. F. Malek, M. Rusop. Sensors Actuat. A-Phys. **171**, 241-247 (2011).
[43] A. Ranga Roa, V. Dutta. Nanotech. **19**, 445712 (2008).
[44] P. Vanlaeke, A. Swinnen, I. Haeldermans, G. Vanhoyland, T. Aernounts, D. Cheyns, C. Deibel, J. D'haen, P. Heremans, J. Poormans, J. V. Manca. Sol. Energy Mater Sol. Cells. **90**, 2150 (2006).